Current Biology ELSEVIER FREE Full-Text Article

Curr Biol. 2020 Oct 19; 30(20): 4103–4111.e6.
doi: 10.1016/j.cub.2020.07.095: 10.1016/j.cub.2020.07.095

PMCID: PMC7575197
PMID: 32857976

Uclacyanin Proteins Are Required for Lignified Nanodomain Formation within Casparian Strips

Guilhem Reyt,[1] Zhenfei Chao,[2] Paulina Flis,[1] Isai Salas-González,[3,4] Gabriel Castrillo,[1] Dai-Yin Chao,[2] and David E. Salt[1,5,*]

[1]Future Food Beacon of Excellence & School of Biosciences, University of Nottingham, Nottingham LE12 5RD, UK
[2]National Key Laboratory of Plant Molecular Genetics, Chinese Academy of Sciences, Center for Excellence in Molecular Plant Sciences, Institute of Plant Physiology and Ecology, Shanghai Institutes for Biological Sciences, Chinese Academy of Sciences, Shanghai, China
[3]Curriculum in Bioinformatics and Computational Biology, Department of Biology, University of North Carolina at Chapel Hill, Chapel Hill, NC, USA
[4]Howard Hughes Medical Institute, University of North Carolina at Chapel Hill, Chapel Hill, NC, USA
David E. Salt: david.salt@nottingham.ac.uk
*Corresponding author david.salt@nottingham.ac.uk
[5]Lead Contact

Received 2020 Apr 29; Revised 2020 Jul 14; Accepted 2020 Jul 28.

Summary

Casparian strips (CSs) are cell wall modifications of vascular plants restricting extracellular free diffusion into and out of the vascular system [1]. This barrier plays a critical role in controlling the acquisition of nutrients and water necessary for normal plant development [2, 3, 4, 5]. CSs are formed by the precise deposition of a band of lignin approximately 2 μm wide and 150 nm thick spanning the apoplastic space between adjacent endodermal cells [6, 7]. Here, we identified a copper-containing protein, Uclacyanin1 (UCC1), that is sub-compartmentalized within the CS. UCC1 forms a central CS nanodomain in comparison with other CS-located proteins that are found to be mainly accumulated at the periphery of the CS. We found that loss-of-function of two uclacyanins (*UCC1* and *UCC2*) reduces lignification specifically in this central CS nanodomain, revealing a nano-compartmentalized machinery for lignin polymerization. This loss of lignification leads to increased endodermal permeability and, consequently, to a loss of mineral nutrient homeostasis.

Keywords: Casparian strips, Uclacyanin, phytocyanin, nanodomain, lignin, extracellular diffusion barriers, endodermis, plant cell wall

Graphical Abstract

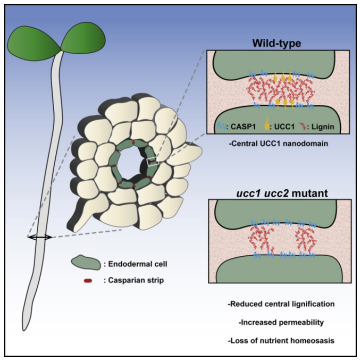

Results and Discussion

Plant roots perform the critical function of controlling the uptake of water and mineral nutrients from the soil essential for plant growth and development. A specialized cell layer in the root called the endodermis plays a key role in the selective uptake of mineral nutrients into the stele for translocation to the shoot [2, 5, 6, 8]. Of vital importance to this function are Casparian strips (CSs), which are belt-like lignin structures surrounding each endodermal cell, that interlock to form a barrier to diffusion in the apoplast [9, 10]. This barrier is thought to enable the endodermis to exert control over uptake of water and solutes from the environment into the plant and perhaps also to control biotic interactions [1, 11].

The precise deposition of lignin for CS formation requires a signaling pathway involving the kinases SGN1 and SGN3 controlling the spatial production of reactive oxygen species (ROS) through the activation of the RBOHF NADPH oxidases [5, 9, 12, 13, 14]. Lignin polymerization requires the localized action of a peroxidase (PER64) [15] and a dirigent-like protein (ESB1) [6]. This biosynthetic machinery is likely placed at the CS deposition site by association with CASPARIAN STRIP MEMBRANE DOMAIN PROTEINS (CASPs) [7]. The CASPs form a highly scaffolded transmembrane domain guiding where the CS forms. Furthermore, the receptor-like kinase SGN3 acts as a sensor of CS integrity by inducing over-lignification of the endodermal cells when the CS is defective [4, 5].

A network of transcriptional factors involving SHR, SCR, and MYB36 controls endodermal differentiation [16, 17]. The MYB36 transcription factor controls the expression of most of the described genes associated with CS formation, including *CASPs*, *ESB1*, and *PER64* [2, 18]. Characterization of other MYB36-regulated genes could thus lead to the identification of new actors involved in CS formation.

Among the genes downregulated in a *myb36* loss-of-function mutant [2, 18], we identified a *Uclacyanin1* gene (*UCC1*) that belongs to the copper-containing phytocyanins family [19] (Figure 1A). This family is divided into three sub-families according to their copper binding amino acid: uclacyanins, stellacyanins, and plantacyanins. The functional role of these proteins remains unknown. However, biophysical and structural data of several phytocyanins suggest their implication in redox reactions with small molecular weight compounds [19, 20, 21, 22, 23, 24]. The expression of several members of this family have been previously shown to be associated with lignified tissues [25, 26, 27]. We looked at the endodermal spatiotemporal expression pattern of the different members of this family (Figure 1A). We found that *UCC1*, *UCC2*, and, to a lesser extent, *UCC8* and *STC1* are expressed in the endodermis similarly to that observed for *CASP1* and *ESB1*. Additionally, UCC1 and UCC2 were found among the top 15 marker genes for endodermal specificity in a single-cell RNA sequencing dataset [28]. Due to the lack of T-DNA insertional mutants in the *UCC1* gene, we generated two loss-of-function mutants, *ucc1.1* and *ucc1.2*, using CRISPR/Cas9 technology (Figure 1B). These mutants bear a single base deletion (*ucc1.1*) and an insertion (*ucc1.2*), leading to shifts in the reading frame in both. For *UCC2* characterization, we used two T-DNA mutants, *ucc2.1* presenting an insertion in the coding sequence (Figure 1B) and *ucc2.2* presenting an insertion in the 3′UTR. The two *ucc1* alleles show a slight although significant delay in formation of an apoplastic barrier, as visualized by the uptake of the apoplastic tracer propidium iodide (PI) after 10 min of staining (Figure 1C). The T-DNA mutants *ucc2.1* and *ucc2.2* did not show an increase of PI permeability. Notably, in *ucc1ucc2* double mutants, with strong reduction in expression of both *UCC1* and *UCC2* in *ucc1.2ucc2.1* (Figure S1A), a strong increase of PI permeability is observed similar to that found in other CS mutants such as *esb1* and *casp1casp3* (Figure S1B). However, the number of cells permeable to PI in *ucc1.2ucc2.1* is highly variable in comparison with *casp1casp3* and *esb1*. When the incubation time with PI is increased to 20 min, *ucc1.2ucc2.1* displays an enhanced permeability in comparison with *esb1*. Taken together, these results highlight the redundant role of UCC1 and UCC2 for establishing a functional apoplastic barrier. No additive effect on PI permeability was observed in the triple mutant *ucc1.1casp1casp3* or in the doubles *ucc1.2esb1* and *ucc1.2sgn3* in comparison with *casp1casp3*, *esb1*, and *sgn3*, respectively (Figure S1B). The loss of CS integrity in *esb1*, *myb36*, and *casp1casp3* is accompanied by an increased deposition of suberin [2, 5, 6] as a compensatory mechanism under the control of SGN3 [4]. We analyzed the pattern of suberin deposition using fluorol yellow 088 staining in the *ucc* mutants (Figure 1D). Deposition of suberin did not increase in the single mutants *ucc1.1*, *ucc1.2*, *ucc2.1*, or *ucc2.2*. However, the double mutant *ucc1.2ucc2.1* induces an increase in endodermal suberization compared with wild-type (WT) plants. This increase is not as strong as that observed in *esb1* or *casp1casp3* (Figure S1C). The combination of *ucc1* mutations in *esb1* and *casp1casp3* do not affect the enhanced suberization of *esb1* or *casp1casp3*.

Disruption of CS is known to affect the composition of the leaf ionome as observed in *esb1*, *myb36*, *casp1casp3*, *sgn3*, and *lotr1* [2, 3, 5, 6]. In order to determine the contribution of UCC1 and UCC2 in maintaining mineral nutrient homeostasis, we analyzed the leaf ionome in different mutant combinations (Figure 1E; Table S1) using inductively coupled plasma mass spectrometry (ICP-MS). The *ucc1* and *ucc2* single mutants have similar leaf ionomes, which group together in a hierarchical clustering (Figure 1E). However, the leaf ionome of the *ucc1.2ucc2.1* double mutant separates from the single mutants,

grouping instead with *esb1*. The leaf ionome of the double mutants *ucc1sgn3* group with the *sgn3* mutant, and the double mutants *ucc1esb1* group with the *esb1* mutant (Figure 1E). This confirms that there is no or little additivity of the leaf ionomic phenotype between *ucc1* and *sgn3* or *esb1*.

The higher endodermal permeability and the atypical ionomic profile observed in the *ucc*(*s*) mutants (Figures 1 and S1) strongly suggest that UCCs play an important role in CS formation. To identify the cell type in which the *UCC1* promoter is activated, we fused the *UCC1* promoter to *GFP* (Figure S2A). GFP was accumulated only in the endodermis, from the elongation zone and further up into the zone of differentiated endodermal cells. According to the literature, the phytocyanin proteins are predicted to be located on the cell surface and anchored to the plasma membrane via a glycosylphosphatidylinositol (GPI) anchor [29]. Several members of this family, including UCC2, have been shown to be GPI-anchored using a proteomic approach [29]. In order to determine the precise UCC1 localization, we generated a line (*pUCC1::mCherry-UCC1*) expressing a tagged UCC1 (Figure 2A). The mCherry-UCC1 fusion accumulates at the endodermal cell junctions where the CS is located (Figure 2B). It first appears in a discontinuous manner in the early stage of endodermal differentiation, and then forms a more continuous band later in the endodermis development.

When we analyzed the localization of mCherry-UCC1 in plants expressing *CASP1-GFP*, we observed a similar pattern of localization at the CS as seen in the maximum projection view of endodermal cells in Figure 2C. However, at higher magnification, in both the median and surface views, we observed mCherry-UCC1 to occupy a more central position in comparison with CASP1-GFP. This was further confirmed using super-resolution structured illumination microscopy (Figure S2B). Moreover, CASP1-GFP does not form a homogeneous domain but is found to accumulate more at the periphery of the CS and less in the center where UCC1 is observed. Subsequently, we checked whether mCherry-UCC1 colocalizes with lignin deposition in the CS (Figure S2C). At the early stage of endodermal differentiation, lignin presents a nearly perfect colocalization with mCherry-UCC1. However, the line expressing mCherry-UCC1 also presents ectopic lignification later in development. This ectopic lignification is similar to that observed in other CS mutants such as *casp1casp3* and *esb1* [6, 7]. Expression of *mCherry-UCC1* in two independent lines also delayed the formation of a functional barrier to PI, and this is not the case for plants expressing the same construct with no mCherry. It also promotes a significant increase of suberin deposition (Figures S2D–S2F). These observations taken together show that expressing *UCC1* with a fluorescent tag in a WT background acts as a dominant negative mutation causing disruption of the CS.

To establish whether the expression of *mCherry-UCC1* can affect the pattern of accumulation of CASP1-GFP presented in Figures 2C and S2B, we examined plants expressing *CASP1-GFP* only (Figure 2D). CASP1-GFP is still more accumulated at the periphery, and this was also observed for another member of the CS machinery ESB1-mCherry. Immunolocalization confirmed that native UCC1 protein is specifically localized to the CS (Figures 2E and S2G). Its CS localization was reduced in *ucc1.2*, further decreased in *ucc1.2ucc2.1* mutants, and abolished in an *myb36* mutant (Figures S2G and S2H). This difference between *ucc1.2* and *ucc1.2ucc2.1* shows that the antibody is promiscuous and able to bind to UCC2, strongly suggesting a CS localization for UCC2. Immunolocalization confirmed our previous observations of a central localization of UCC1 in the CS as compared with CASP1-GFP (Figure 2E). Quantification of pixel intensity across the CS reveals that UCC1 is highly accumulated in the middle of the CS, where CASP1-GFP is less accumulated compared with the periphery of the CS domain (Figure 2F). The CASP1 domain of the plasma membrane is defined as a microdomain [30] as its width is around 1.5 μm. UCC1 with a more central accumulation has a width equal or slightly smaller than 1 μm, UCC1 can then be classified as a nanodomain of the CS. This subdomain structure has not been previously reported. However, previous studies for CASP1, ESB1, and PER64 [7, 31] do appear to show an enrichment of these proteins at the periphery of the CS. This means that the level of organization observed at the plasma membrane for CASP1 is conserved for cell wall proteins such as ESB1 and PER64. To date, UCC1 is the only protein found in the central nanodomain of the CS, revealing a new level of internal structure within the CS.

To characterize the formation of the UCC1 and CASP1 subdomains, we tracked endodermal differentiation cell-by-cell. CASP1-GFP and mCherry-UCC1 are found to be accumulated in the endodermis concomitantly between 4 and 6 cells after the onset of elongation, at the periphery of the cells and not yet at the CS (Figures 3A and 3B), which is consistent with a common transcriptional regulation by MYB36. We then tracked the central accumulation of CASP1-GFP and mCherry-UCC1 at the CS. We observed that the localization of CASP1-GFP and mCherry-UCC1 at the CS mainly occurs at the eighth endodermal cell after the onset of elongation (Figure 3B). However, mCherry-UCC1, but not CASP1-GFP, was observed to be centrally localized in several independent events at the seventh cell after the onset of elongation. This suggests that CASP1 localization at the CS is not required for the recruitment of UCC1. This was further confirmed by the normal accumulation of UCC1 at the CS in a *casp1casp3* mutant (Figures 3C and S3A). However, UCC1 is not able to form a continuous domain in *casp1casp3* as in WT. This was also observed in the *esb1*, *sgn3*, and *esb1sgn3* mutants. We then tested the reciprocity to know whether UCC1 and UCC2 are required for CASP1-GFP localization (Figure 3D). In the *ucc1.1* and *ucc1.1ucc2.1* mutants, CASP1-GFP is able to localize at the CS domain and form a continuous domain without disruption. This demonstrates that

UCC1 and UCC2 are not required for CASP1 localization to the CS domain. However, the absence of UCC1 and UCC2 does affect CASP1-GFP localization at a nanoscale resolution (Figures 3E and 3F). The exclusion of CASP1-GFP from the central nanodomain of the CS is reduced in the *ucc1* mutants and tends to disappear in the double *ucc1.1ucc2.1* mutant. This indicates a role for UCC1 and UCC2 in the formation of the central CS nanodomain. We then tested whether ROS production and lignin polymerization are required for the exclusion of CASP1-GFP from the central nanodomain. We observed that CASP1-GFP is still more accumulated at the periphery of the CS when ROS production is abolished in a *rbohf* mutant (Figures S3B and S3C) [12, 15] and when lignin polymerization is prevented using piperonilyc acid, an inhibitor of the phenylpropanoid pathway [10, 32]. This suggests a direct role for UCC1 and UCC2 in excluding CASP1-GFP from the central nanodomain of the CS.

Knowing that UCC1 localizes at the CS (Figures 2C–2F) and mutations in *UCC1* and *UCC2* cause a strong defect in root apoplastic permeability (Figures 1C and S1B), we looked at lignin deposition at the CS in *ucc1&2* mutants (Figure S4A). Mutations in *UCC1* and/or *UCC2* do not cause an obvious disruption in the CS as observed in *casp1casp3*, *esb1*, *sgn3* (Figure S4A), and other previously identified CS mutants, where clear gaps can be observed [3, 5, 6, 7, 11, 13, 14, 15, 33]. Further, there is no additivity between *ucc1*, *esb1*, and *casp1casp3* observed for the deposition of ectopic lignin (Figure S4A). Importantly, mutations in *UCC1* do reduce the amount of lignin in the central nanodomain of the CS, as observed using confocal imaging (Figure 4A), and super-resolution structured illumination microscopy (Figure 4B). Pixel quantification across the CS reveals that *ucc1* mutants show a lower lignification in the central nanodomain (Figure 4B) where UCC1 accumulates (Figures 2C–2F). This decrease is not observed in *ucc2.1*. A further decrease is observed in the double mutant *ucc1.2ucc2.1* in comparison with *ucc1* mutants. This is consistent with the increased root permeability observed in *ucc1.2ucc2.1* in comparison with the single mutants (Figures 1C and S1B). This reveals that CS permeability can be strongly affected in the absence of clear gaps in the CS. Furthermore, we observed ectopic lignification on the cortical side of the endodermis on a few occasions in the *ucc1* mutants and at a higher frequency in the double mutant *ucc1.2ucc2.1* (Figures 4A, 4B, and S4). This is a typical phenotype, along with increased suberin deposition, that is due to the SGN3-dependent compensatory mechanism observed in most mutants with defective CS [2, 5, 6, 7, 12]. However, the ectopic lignification and enhanced suberization are observed to a lesser degree in *ucc1.2ucc2.1* in comparison with other CS mutants such as *casp1casp3* and *esb1* mutants (Figures 1D, 4, S1C, and S4). This could be explained by a more conditional leakiness of the CS in *ucc1ucc2* mutants. Discontinuities below the resolution of light microscopy could occur in *ucc1ucc2* mutants. This could lead to a full permeability for low molecular weight compounds, such as ions and PI, but an intermediate permeability for high molecular weight compounds, such as the CIF peptides required for ectopic lignification and enhanced suberization [13, 14].

In conclusion, this study reveals the first loss-of-function phenotype for members of the plant-specific blue copper protein family of phytocyanins. Several studies suggested their implication in lignin polymerization [25, 26, 27], but this has never previously been shown. Our analysis indicates a role for the uclacyanins in the deposition of lignin in a newly discovered nanoscale domain within the CS. Further, the subcellular localization of UCC1, and the phenotype of the *ucc*(*s*) mutants, reveals a sub-compartmentalization of the machinery required for lignin polymerization at the CS.

STAR★Methods

Key Resources Table

Resource Availability

Lead Contact Further information and requests for resources and reagents should be directed to and will be fulfilled by the Lead Contact, David E Salt (David.Salt@nottingham.ac.uk).

Material Availability Materials from this study are available on request.

Data and Code Availability This study did not generate or ANALYZE datasets or code.

Experimental Model and Subject Details

Plant material *Arabidopsis thaliana* ecotype Columbia (Col_0) and the following mutants and transgenic lines were used in this study: *ucc1.1* (this study), *ucc1.2* (this study), *sgn3* (*sgn3.3*; SALK_043282 [5]), *myb36* (*myb36.2*; GK-543B11 [2]), *casp1 casp3* (*casp1.1 casp3.1* [7]), *pCASP1::CASP1-GFP* [7], *pESB1::ESB1-mCherry* [6], *ucc2.1* (GK_250F04), *ucc2.2* (salk_049638) and *rbohf* (salk_059888 [15]).

The corresponding gene AGI are: *UCC1*, AT2G32300; *UCC2*, AT2G44790;

SGN3, At4g20140; *MYB36*, At5g57620; *CASP1*, At2g36100; *CASP3*, AT2G27370;

ESB1, At2g28670; *RBOHF*, At1g64060.

Growth Conditions All seeds were surface sterilized, and then stratified for two days at 4°C. Seeds were directly germinated on plates containing MS medium (Murashige and Skoog, Sigma) solidified with 0.8% agar, pH 5.7, and grown in a vertical position in a growth chamber under long-day conditions (16 h light 22°C/8 h dark 19°C, light intensity 100µE). The lignin biosynthesis inhibitor piperonylic acid (PA, Sigma Aldrich) was used at the concentration of 10 µM from germination. Seedlings were analyzed at 6-day-old for microscopy analysis, and 2-week-old for ionomic analysis.

Method Details

Generation of transgenic lines and CRISPR/Cas9 mutants The line *pUCC1::mCherry-UCC1* was obtained using Gateway Cloning Technology (Invitrogen). A genomic DNA fragment containing the *UCC1* promoter (−3083bp before ATG), the UCC1 5′UTR and the UCC1 signal peptide (+78bp after ATG) was amplified by PCR using the following primers: F: GGGGACAACTTTGTATAGAAAAGTTG**GTTGAATTTCGTAAGAGTTAGG** and R: GGGGACTGCTTTTTTGTACAAACTTGC**ATGGTCAGTAGCTACTGTTAAACC**; and cloned in a pDONR P4-P1R. A second fragment containing the rest of the genomic UCC1 sequence (from +79 to +1081 from ATG) was amplified by PCR with the primers: F: GGGGACAGCTTTCTTGTACAAAGTGGTA**ACCATTGGTGGTCCTAGTGGTTGG** and R: GGGGACAACTTTGTATAATAAAGTTGA**CCCATATAAATTGTAATAATGTATTATAAAC** and cloned in a pDONR P2R-P3. Both fragments and a pEN-L1-mCherry-L2 vector were assembled in the expression vector pB7m34GW [34].

The line pUCC1::UCC1 was obtained using Gateway Cloning Technology. A genomic DNA fragment containing the *UCC1* promoter (−3083bp before ATG) was amplified by PCR using the following primers: F: GGGGACAACTTTGTATAGAAAAGTTG**GTTGAATTTCGTAAGAGTTAGG** and R: GGGGACTGCTTTTTTGTACAAACTTGG**ATGACATATGGTGTCAAATGTGTG**; and cloned in a pDONOR P4-P1R. A second fragment containing the genomic UCC1 sequence was amplified by PCR with the primers: GGGGACAAGTTTGTACAAAAAAGCAGGCTCG**GCACAAAACATCATCATCTCTTG** and R: GGGGACCACTTTGTACAAGAAAGCTGGGT**CCCATATAAATTGTAATAATGTATTATAAAC**; and cloned in a pDONOR P1-P2. Both fragments and a vector were assembled in the expression vector pH7m24GW.

The construct *pUCC1::GFP-GUS* was generated using Gateway cloning technology. The *UCC1* promoter (−3083bp to −83bp before ATG) was amplified by PCR with these primers: F: GGGGACAAGTTTGTACAAAAAAGCAGGCT**GTTGAATTTCGTAAGAGTTAGG; Primer R:** GGGGACCACTTTGTACAAGAAAGCTGGGT**ATGACATATGGTGTCAAATGTGTG** and cloned in pBGWFS7 [35].

Following Agrobacterium strain GV3101 transformation with the resulting vector, transgenic plants were generated by floral dipping [39].

The *ucc1.1* and *ucc1.2* mutants were obtained using CRISPR/Cas9 according to [36]. Two sgRNA targeting *UCC1* coding sequence (GTCCTCGCTACTACACTCA and GGTCCTAGTGGTTGGACTG) were inserted in to the pHEE401 vector following Agrobacterium strain GV3101 transformation with the resulting vector, transgenic plants were generated by floral dipping [39]. Two individual homozygous lines (*ucc1.1*; *ucc1.2*) were identified at the generation T1.

Phylogeny A BLASTP was performed using UCC1 amino acid sequence against the Araport11 protein sequences dataset [40]. Only the matches with an Expect value (E-value) lower than 0.05 were considered. A first alignment was performed to select the protein sequence containing the amino acid required for copper binding as described in [19]. Genes were named and classified as stellacyanin, uclacyanin and plantacyanin according to the amino acid binding copper as described in [41]. A second alignment and tree assembling were performed using Clustal Omega with amino acid sequence of the putative copper containing protein [42].

Endodermal spatio-temporal expression pattern The spatio-temporal endodermal expression pattern of the corresponding genes was checked using the Bio-Analytic Resource database from the AtGenExpress Consortium [43].

Gene expression analysis The plants were grown for 6 days on 1/2 M/S plates. Seeds were sown in three parallel lines per square plates (12*12 cm) at high density. The first 5 mm of root tips were collected. One plate was used as a biological replicate. The samples were snap-frozen at harvest and ground into fine powder in a 2 mL centrifuge tube. Total RNA was extracted according to [44]. Samples were homogenized in 400 µL of Z6-buffer containing 8 M guanidine-HCl, 20 mM MES, 20 mM EDTA pH 7.0 After the addition of 400 µl phenol:chloroform:isoamylalcohol, 25:24:1, samples were vortexed and centrifuged (15,000 g 10 min.) for phase separation. The aqueous phase was transferred to a new 1.5 mL tube and 0.05 volumes of 1 N acetic acid qnd 0.7 volumes 96% ethanol was added. The RNA was precipitated at −20°C overnight. Following centrifugation (15,000 g 10 min, 4°C), the pellet was washed with 200µL 3M sodium acetate at pH 5.2 and 70% ethanol. The RNA was dried and dissolved in 30 µL of ultrapure water and store at −80°C until use. DNase treatment (DNase

I, Amplification Grade, 18068015, Invitrogen) was carried out on the samples to remove genomic DNA. The RNA Concentration and quality were determined using Qubit (Invitrogen; Q10210) and TapeStation (Agilent; G2991A) protocols. Librairies were generated using the Lexogen Quant Seq 3′ mRNA Seq (FWD) Library Prep Kit (Lexogen; 015) which employs polyA selection to enrich for mRNA. Library yield was measured by Qubit (Invitrogen; Q10210) and TapeStation (Agilent; G2991A) systems. protocols to determine concentration and library size, these are then pooled together in equimolar concentrations. The concentration of the pool of libraries were confirmed using the Qubit and qPCR and then loaded onto an Illlumina NextSeq 500 on a NextSeq 500/550 High Output Kit v2.5 (75 Cycles) (Illumina; 20024906), to generate approximately 5 million 75bp single-end reads per sample.

Initial quality assessment of the Illumina RNA-Seq reads was performed using FastQC v0.11.8. (Babraham Bioinformatics, Cambridge, UK). Trimmomatic v0.36 was used to identify and RNA-Seq read processing discard reads containing the Illumina adaptor sequence [45]. The resulting high-quality reads were then mapped against the TAIR10 *Arabidopsis* reference genome using HISAT2 v2.1.0 with default parameters [46]. The featureCounts function from the Subread package was then used to count reads that mapped to each one of the 27,206 nuclear protein-coding genes.

To visualize the expression of the different genes sets we applied the DESeq2 v.1.24.0 package variance stabilizing transformation to the raw count gene matrix [47]. We then standardized each gene along the samples to generate a standardized matrix. This standardized matrix was used to visualize the expression of genes across the genotypes assayed. Boxplot of expressions were constructed using the R package ggplot2 [48].

Ionome analysis The shoot elemental content was measured using Inductively Coupled Plasma Mass Spectrometry (ICP-MS) and the analysis was performed as described [49]. Briefly, shoots of 2-week-old plants grown on agar plates were harvested into Pyrex test tubes (16 × 100 mm) to be then dried at 88°C for 20 h. After weighing the appropriate number of samples (these weights were used to calculate the weights of rest of the sample), the trace metal grade nitric acid Primar Plus (Fisher Chemicals) spiked with indium internal standard was added to the tubes (1 mL per tube). The samples were then digested in a dry block heater (DigiPREP MS, SCP Science; QMX Laboratories, Essex, UK) at 115°C for 4 h. The digested samples were diluted to 10 mL with 18.2 MΩcm Milli-Q Direct water (Merck Millipore). Elemental analysis was performed using an ICP-MS, PerkinElmer NexION 2000 equipped with Elemental Scientific Inc. autosampler, in the collision mode (He). Twenty-three elements (Li, B, Na, Mg, P, S, K, Ca, Mn, Fe, Co, Ni, Cu, Zn, As, Rb, Sr, Mo, Cd) were monitored. Liquid reference material composed of pooled samples was prepared before the beginning of sample run and was used throughout the whole samples run. It was run after every ninth sample to correct for variation within ICP-MS analysis run. The calibration standards (with indium internal standard and blanks) were prepared from single element standards (Inorganic Ventures; Essex Scientific Laboratory Supplies Ltd, Essex, UK) solutions. Sample concentrations were calculated using external calibration method within the instrument software. Further data processing was performed using Microsoft Excel spreadsheet.

Histological staining of roots Propidium iodide (PI) staining was performed as previously described [9]. 6day-old seedlings were incubated in 15 μM propidium iodide for 10 min in the dark, then incubated in water for 30 s, mounted in water using a slide and coverslip and immediately observed with microscope. Block of PI in the endodermis was quantified as the number of endodermal cells after onset of elongation. Onset of elongation was defined as the point where the length of an endodermal cell was more than twice its width.

Root clearing and staining with Calcofluor White, Basic Fuchsin and Auramine-O was performed using Clearsee solution according to [50]. Six-day old seedlings were fixed with 4% PFA for 60–120 min at 20°C. Seedlings were then washed twice for 1 min in 1x PBS and moved to the Clearsee solution (10% xylitol, 15% Sodium deoxycholate, 25% urea). For Basic Fuchsin staining, the seedlings were stained overnight in 0.2% Basic Fuchsin prepared in ClearSee. The next day, Basic Fuchsin solution was removed and the seedlings were washed twice for 60 min in ClearSee with gentle shaking. Auramine-O staining (0.1% in Clearsee) was performed as for Basic Fuchsin. For Calcofluor White staining, the seedlings were stained for 30 min in 0.1% Calcofluor White in ClearSee solution. The seedlings were washed twice in ClearSee for 30 min.

Fluorol Yellow 088 staining of the suberin was performed as previously described [8, 10]. Seedlings were incubated in Fluorol Yellow 088 (0.01%w/v, lactic acid) at 70°C for 30 min, rinsed with water and counterstained with aniline blue (0.5% w/v, water) at RT for 30 min in darkness, washed with water, and observed with a microscope.

UCC1 immunolocalization Custom affinity-purified polyclonal anti-UCC1 antibodies were produced by Genscript, USA and were used as a primary antibody. Anti-UCC1 antibodies were generated in rabbits against a recombinant truncated UCC1 (TDHTIGGPSGWTVGASLRTWAAGQTFAVGDNLVFSYPAAFHD VVEVTKPEFDSCQAVKPLITFANGNSLVPLTTPGKRYFICGMPGHCSQGMKLEVNVVPTATVAPTA) produced in *E. coli*.

UCC1-immunolocalization was performed according to [51]. 6-day-old seedlings were vacuum infiltrated and fixed with 2% formaldehyde in MTSB buffer (microtubule-stabilizing buffer) supplemented with 0.1% Triton for 1 h. A stock solution of 2x MTSB was prepared with: 15 g PIPES, 1.90 g EGTA, 1.22 g $MgSO_4 \cdot 7H_2O$ and 2.5 g KOH and dissolved in a total volume of 500 mL water at pH 7.0 (adjusted with 10 M KOH). Seedlings were washed twice in water that was then replaced by 100% methanol. Methanol content in the wash was gradually decreased until its final concentration reached ~20%. Seedlings were then washed twice in water and incubated in a cell wall digestion solution (0.2% Driselase, 0.15% Macerozyme in 2mM MES, pH 5.0) for 30 min at 37°C. After washing with MTSB buffer, the seedlings were incubated in a solution containing 3% IGEPAL CA-630, 10% DMSO in MTSB buffer for 15min at 37°C in order to permeabilize the cell membranes. Seedling were then washed 4 times with MTSB buffer and blocked using a blocking solution containing 2% albumin fraction V BSA in MTSB buffer for 20 min at room temperature. The primary anti-UCC1 antibody was diluted (1/500) in the blocking solution and added to the seedlings for 1 h incubation at 37°C.Then seedlings were washed twice with MTSB buffer and incubated with the secondary antibody goat anti-Rabbit IgG DyLight 633 (Invitrogen) in MTSB buffer for 1 h at 37°C. After washing three times in MTSB buffer, the seedlings were mounted on microscopic slides in MTSB buffer for the microscopy analysis. Antibody specificity was tested on *myb36*, *ucc1.2* and *ucc1.2ucc2.1* mutants and by using no primary antibody as a negative control. Pixel intensity quantification was performed along a 1.2 µm-wide line following the CS (defined as Dylight 633 signal) in WT, *ucc1.2* and *ucc1.2 ucc2 using* Fiji. For "No primary Ab" control and *myb36*, pixel intensity was measures in the endodermal cells at random locations due to the absence of visible CS.

Microscopy Laser scanning confocal microscopy was performed with a Zeiss LSM500 and a Leica SP8. Structured illumination microscopy was performed with a Zeiss PS1 Super Resolution Microscope. The following excitation and emission detection settings were applied: Calcofluor White, 405 nm/425-475 nm; GFP, 488 nm/500-550 nm; Fluorol yellow 088, 488 nm/500-550 nm; Auramine-O 488nm/505-530nm; propidium iodide, 561 nm/600-620 nm; Basic Fuchsin, 561 nm/570-650 nm; mCherry, 561 nm/ 570-620 nm; Dylight 633, 633 nm/640-670 nm.

Pixel intensity quantification across the Casparian strip Images of CS surface view were analyzed for *CASP1-GFP*, lignin (Basic fuchsin*), mCherry-UCC1* and DyLight 633 using Fiji [37]. A segmented line with a width of at least 3.8 µm was traced along the central part of the CS. This selection was then straighten using the "Straighten…" function. A profile of pixels intensity along the y axis was then generated from the pericycle side toward the cortical side. Each replicate represents the average value of pixels intensity across 13 µm approximately and it was generated from one picture. The pixels intensity values were normalized to compare the profile of pixel intensity across the different pictures. The intensity values were scaled from 0 to 1 using the following formula: $(x\text{-}x_{MIN})/(x_{MAX}\text{-}x_{MIN})$. In order to obtain a normalization based solely on CS signal and not on ectopic lignification, the values corresponding to ectopic lignification were intentionally omitted, in the cases the fluorescence signal intensity coming from ectopic lignification (corner of the endodermal cells) was higher than the one coming from the CS itself in the single picture. The profiles of normalized pixel intensity were plotted using PlotTwist [38] and RStudio. Statistical analysis was performed on normalized data in the ranges defined in the figures.

Timing of expression and localization of CASP1 and UCC1 The timing of CASP1 and UCC1 accumulation and localization at the CS domain were quantified as number of cells after the onset of elongation as previously described [31, 33]. The cell number for the endodermal accumulation of CASP1 and UCC1 was determined in the first cell after the onset of elongation where GFP or mCherry signal were detectable using confocal microscopy.

Quantification and Statistical Analysis

For all the experiments, detail of statistical tests used and error-bars on barplots are indicated in the figure legends.

Acknowledgments

We thank Dr. Robert Markus (Super Resolution Microscopy Facility, University of Nottingham), the Microscopy and Histology Facility of the University of Aberdeen, and John Danku for ICP-MS analysis. We thank Dr. Inês Barbosa and Prof. Niko Geldner for critical reading of the manuscript. This work was supported by grants from the UK Biotechnology and Biological Sciences Research Council grant (BB/N023927/1 to D.E.S.), the Coordinating Action in Plant Sciences promoting sustainable collaboration in plant sciences (ERACAPS13.089_RootBarriers to D.E.S.), and a Future Food Beacon of Excellence Nottingham Research Fellowship to G.C.

Author Contributions

Conceptualization, G.R., G.C., and D.E.S.; Formal Analysis, G.R. and I.S.-G.; Investigation, G.R., Z.C., P.F., and G.C.; Methodology, G.R. and Z.C.; Writing – Original Draft, G.R.; Writing – Review & Editing G.R., Z.C., P.F., G.C., D.-Y.C., and D.E.S.; Supervision, D.E.S.

Declaration of interests

The authors declare no competing interests.

Notes

Published: August 27, 2020

Footnotes

Supplemental Information can be found online at https://doi.org/10.1016/j.cub.2020.07.095.

Supplemental Information

Document S1. Figures S1–S4 and Table S1:

Document S2. Article plus Supplemental Information:

References

1. Geldner N. The endodermis. Annu. Rev. Plant Biol. 2013;64:531–558. [PubMed: 23451777]

2. Kamiya T., Borghi M., Wang P., Danku J.M.C., Kalmbach L., Hosmani P.S., Naseer S., Fujiwara T., Geldner N., Salt D.E. The MYB36 transcription factor orchestrates Casparian strip formation. Proc. Natl. Acad. Sci. USA. 2015;112:10533–10538. [PMCID: PMC4547244] [PubMed: 26124109]

3. Li B., Kamiya T., Kalmbach L., Yamagami M., Yamaguchi K., Shigenobu S., Sawa S., Danku J.M.C., Salt D.E., Geldner N., Fujiwara T. Role of LOTR1 in Nutrient Transport through Organization of Spatial Distribution of Root Endodermal Barriers. Curr. Biol. 2017;27:758–765. [PubMed: 28238658]

4. Wang P., Calvo-Polanco M., Reyt G., Barberon M., Champeyroux C., Santoni V., Maurel C., Franke R.B., Ljung K., Novák O. Surveillance of cell wall diffusion barrier integrity modulates water and solute transport in plants. Sci. Rep. 2019;9:4227. [PMCID: PMC6414709] [PubMed: 30862916]

5. Pfister A., Barberon M., Alassimone J., Kalmbach L., Lee Y., Vermeer J.E., Yamazaki M., Li G., Maurel C., Takano J. A receptor-like kinase mutant with absent endodermal diffusion barrier displays selective nutrient homeostasis defects. eLife. 2014;3:e03115. [PMCID: PMC4164916] [PubMed: 25233277]

6. Hosmani P.S., Kamiya T., Danku J., Naseer S., Geldner N., Guerinot M.L., Salt D.E. Dirigent domain-containing protein is part of the machinery required for formation of the lignin-based Casparian strip in the root. Proc. Natl. Acad. Sci. USA. 2013;110:14498–14503. [PMCID: PMC3761638] [PubMed: 23940370]

7. Roppolo D., De Rybel B., Dénervaud Tendon V., Pfister A., Alassimone J., Vermeer J.E.M., Yamazaki M., Stierhof Y.-D., Beeckman T., Geldner N. A novel protein family mediates Casparian strip formation in the endodermis. Nature. 2011;473:380–383. [PubMed: 21593871]

8. Barberon M., Vermeer J.E.M., De Bellis D., Wang P., Naseer S., Andersen T.G., Humbel B.M., Nawrath C., Takano J., Salt D.E., Geldner N. Adaptation of Root Function by Nutrient-Induced Plasticity of Endodermal Differentiation. Cell. 2016;164:447–459. [PubMed: 26777403]

9. Alassimone J., Naseer S., Geldner N. A developmental framework for endodermal differentiation and polarity. Proc. Natl. Acad. Sci. USA. 2010;107:5214–5219. [PMCID: PMC2841941] [PubMed: 20142472]

10. Naseer S., Lee Y., Lapierre C., Franke R., Nawrath C., Geldner N. Casparian strip diffusion barrier in Arabidopsis is made of a lignin polymer without suberin. Proc. Natl. Acad. Sci. USA. 2012;109:10101–10106. [PMCID: PMC3382560] [PubMed: 22665765]

11. Durr J., Reyt G., Spaepen S., Hilton S., Meehan C., Qi W., Kamiya T., Flis P., Dickinson H.G., Feher A. Two Receptor-Like Kinases Required For Arabidopsis Endodermal Root Organisation Shape The Rhizosphere Microbiome. bioRxiv. 2019 doi: 10.1101/816330. [CrossRef: 10.1101/816330]

12. Fujita S., De Bellis D., Edel K.H., Köster P., Andersen T.G., Schmid-Siegert E., Dénervaud Tendon V., Pfister A., Marhavý P., Ursache R. SCHENGEN receptor module drives localized ROS production and lignification in plant roots. EMBO J. 2020;39:e103894. [PMCID: PMC7196915] [PubMed: 32187732]

13. Doblas V.G., Smakowska-Luzan E., Fujita S., Alassimone J., Barberon M., Madalinski M., Belkhadir Y., Geldner N. Root diffusion barrier control by a vasculature-derived peptide binding to the SGN3 receptor. Science. 2017;355:280–284. [PubMed: 28104888]

14. Nakayama T., Shinohara H., Tanaka M., Baba K., Ogawa-Ohnishi M., Matsubayashi Y. A peptide hormone required for Casparian strip diffusion barrier formation in Arabidopsis roots. Science. 2017;355:284–286. [PubMed: 28104889]

15. Lee Y., Rubio M.C., Alassimone J., Geldner N. A mechanism for localized lignin deposition in the endodermis. Cell. 2013;153:402–412. [PubMed: 23541512]

16. Li P., Yu Q., Gu X., Xu C., Qi S., Wang H., Zhong F., Baskin T.I., Rahman A., Wu S. Construction of a Functional Casparian Strip in Non-endodermal Lineages Is Orchestrated by Two Parallel Signaling Systems in Arabidopsis thaliana. Curr. Biol. 2018;28:2777–2786.e2. [PubMed: 30057307]

17. Drapek C., Sparks E.E., Marhavy P., Taylor I., Andersen T.G., Hennacy J.H., Geldner N., Benfey P.N. Minimum requirements for changing and maintaining endodermis cell identity in the Arabidopsis root. Nat. Plants. 2018;4:586–595. [PMCID: PMC6135099] [PubMed: 30061749]

18. Liberman L.M., Sparks E.E., Moreno-Risueno M.A., Petricka J.J., Benfey P.N. MYB36 regulates the transition from proliferation to differentiation in the Arabidopsis root. Proc. Natl. Acad. Sci. USA. 2015;112:12099–12104. [PMCID: PMC4593085] [PubMed: 26371322]

19. Nersissian A.M., Immoos C., Hill M.G., Hart P.J., Williams G., Herrmann R.G., Valentine J.S. Uclacyanins, stellacyanins, and plantacyanins are distinct subfamilies of phytocyanins: plant-specific mononuclear blue copper proteins. Protein Sci. 1998;7:1915–1929. [PMCID: PMC2144163] [PubMed: 9761472]

20. Guss J.M., Merritt E.A., Phizackerley R.P., Hedman B., Murata M., Hodgson K.O., Freeman H.C. Phase determination by multiple-wavelength x-ray diffraction: crystal structure of a basic “blue” copper protein from cucumbers. Science. 1988;241:806–811. [PubMed: 3406739]

21. Guss J.M., Merritt E.A., Phizackerley R.P., Freeman H.C. The structure of a phytocyanin, the basic blue protein from cucumber, refined at 1.8 A resolution. J. Mol. Biol. 1996;262:686–705. [PubMed: 8876647]

22. Battistuzzi G., Borsari M., Loschi L., Sola M. Redox thermodynamics, acid-base equilibria and salt-induced effects for the cucumber basic protein. General implications for blue-copper proteins. JBIC. 1997;2:350–359.

23. Nersissian A.M., Mehrabian Z.B., Nalbandyan R.M., Hart P.J., Fraczkiewicz G., Czernuszewicz R.S., Bender C.J., Peisach J., Herrmann R.G., Valentine J.S. Cloning, expression, and spectroscopic characterization of Cucumis sativus stellacyanin in its nonglycosylated form. Protein Sci. 1996;5:2184–2192. [PMCID: PMC2143280] [PubMed: 8931137]

24. Hart P.J., Nersissian A.M., Herrmann R.G., Nalbandyan R.M., Valentine J.S., Eisenberg D. A missing link in cupredoxins: crystal structure of cucumber stellacyanin at 1.6 A resolution. Protein Sci. 1996;5:2175–2183. [PMCID: PMC2143285] [PubMed: 8931136]

25. Drew J.E., Gatehouse J.A. Isolation and characterization of a pea pod cDNA encoding a putative blue copper protein correlated with lignin deposition. J. Exp. Bot. 1994;45:1873–1884.

26. Sterky F., Regan S., Karlsson J., Hertzberg M., Rohde A., Holmberg A., Amini B., Bhalerao R., Larsson M., Villarroel R. Gene discovery in the wood-forming tissues of poplar: analysis of 5, 692 expressed sequence tags. Proc. Natl. Acad. Sci. USA. 1998;95:13330–13335. [PMCID: PMC23802] [PubMed: 9789088]

27. Allona I., Quinn M., Shoop E., Swope K., St Cyr S., Carlis J., Riedl J., Retzel E., Campbell M.M., Sederoff R., Whetten R.W. Analysis of xylem formation in pine by cDNA sequencing. Proc. Natl. Acad. Sci. USA. 1998;95:9693–9698. [PMCID: PMC21401] [PubMed: 9689143]

28. Shulse C.N., Cole B.J., Ciobanu D., Lin J., Yoshinaga Y., Gouran M., Turco G.M., Zhu Y., O’Malley R.C., Brady S.M., Dickel D.E. High-Throughput Single-Cell Transcriptome Profiling of Plant Cell Types. Cell Rep. 2019;27:2241–2247. [PMCID: PMC6758921] [PubMed: 31091459]

29. Borner G.H.H., Lilley K.S., Stevens T.J., Dupree P. Identification of glycosylphosphatidylinositol-anchored proteins in Arabidopsis. A proteomic and genomic analysis. Plant Physiol. 2003;132:568–577. [PMCID: PMC166998] [PubMed: 12805588]

30. Ott T. Membrane nanodomains and microdomains in plant-microbe interactions. Curr. Opin. Plant Biol. 2017;40:82–88. [PubMed: 28865975]

31. Kalmbach L., Hématy K., De Bellis D., Barberon M., Fujita S., Ursache R., Daraspe J., Geldner N. Transient cell-specific EXO70A1 activity in the CASP domain and Casparian strip localization. Nat. Plants. 2017;3:17058. [PubMed: 28436943]

32. Schalk M., Cabello-Hurtado F., Pierrel M.A., Atanossova R., Saindrenan P., Werck-Reichhart D. Piperonylic acid, a selective, mechanism-based inactivator of the trans-cinnamate 4-hydroxylase: A new tool to control the flux of metabolites in the phenylpropanoid pathway. Plant Physiol. 1998;118:209–218. [PMCID: PMC34858] [PubMed: 9733540]

33. Alassimone J., Fujita S., Doblas V.G., van Dop M., Barberon M., Kalmbach L., Vermeer J.E.M., Rojas-Murcia N., Santuari L., Hardtke C.S., Geldner N. Polarly localized kinase SGN1 is required for Casparian strip integrity and positioning. Nat. Plants. 2016;2:16113. [PubMed: 27455051]

34. Karimi M., De Meyer B., Hilson P. Modular cloning in plant cells. Trends Plant Sci. 2005;10:103–105. [PubMed: 15749466]

35. Karimi M., Inzé D., Depicker A. GATEWAY vectors for Agrobacterium-mediated plant transformation. Trends Plant Sci. 2002;7:193–195. [PubMed: 11992820]

36. Wang Z.-P., Xing H.-L., Dong L., Zhang H.-Y., Han C.-Y., Wang X.-C., Chen Q.-J. Egg cell-specific promoter-controlled CRISPR/Cas9 efficiently generates homozygous mutants for multiple target genes in Arabidopsis in a single generation. Genome Biol. 2015;16:144. [PMCID: PMC4507317] [PubMed: 26193878]

37. Schindelin J., Arganda-Carreras I., Frise E., Kaynig V., Longair M., Pietzsch T., Preibisch S., Rueden C., Saalfeld S., Schmid B. Fiji: an open-source platform for biological-image analysis. Nat. Methods. 2012;9:676–682. [PMCID: PMC3855844] [PubMed: 22743772]

38. Goedhart J. PlotTwist: A web app for plotting and annotating continuous data. PLoS Biol. 2020;18 e3000581–e10. [PMCID: PMC6980690] [PubMed: 31929523]

39. Clough S.J., Bent A.F. Floral dip: a simplified method for Agrobacterium-mediated transformation of Arabidopsis thaliana. Plant J. 1998;16:735–743. [PubMed: 10069079]

40. Cheng C.-Y., Krishnakumar V., Chan A.P., Thibaud-Nissen F., Schobel S., Town C.D. Araport11: a complete reannotation of the Arabidopsis thaliana reference genome. Plant J. 2017;89:789–804. [PubMed: 27862469]

41. Nersissian A.M., Shipp E.L. Blue copper-binding domains. Adv. Protein Chem. 2002;60:271–340. [PubMed: 12418180]

42. Madeira F., Park Y.M., Lee J., Buso N., Gur T., Madhusoodanan N., Basutkar P., Tivey A.R.N., Potter S.C., Finn R.D., Lopez R. The EMBL-EBI search and sequence analysis tools APIs in 2019. Nucleic Acids Res. 2019;47(W1):W636–W641. [PMCID: PMC6602479] [PubMed: 30976793]

43. Toufighi K., Brady S.M., Austin R., Ly E., Provart N.J. The Botany Array Resource: e-Northerns, Expression Angling, and promoter analyses. Plant J. 2005;43:153–163. [PubMed: 15960624]

44. Logemann J., Schell J., Willmitzer L. Improved method for the isolation of RNA from plant tissues. Anal. Biochem. 1987;163:16–20. [PubMed: 2441623]

45. Bolger A.M., Lohse M., Usadel B. Trimmomatic: a flexible trimmer for Illumina sequence data. Bioinformatics. 2014;30:2114–2120. [PMCID: PMC4103590] [PubMed: 24695404]

46. Kim D., Paggi J.M., Park C., Bennett C., Salzberg S.L. Graph-based genome alignment and genotyping with HISAT2 and HISAT-genotype. Nat. Biotechnol. 2019;37:907–915. [PMCID: PMC7605509] [PubMed: 31375807]

47. Love M.I., Huber W., Anders S. Moderated estimation of fold change and dispersion for RNA-seq data with DESeq2. Genome Biol. 2014;15:550. [PMCID: PMC4302049] [PubMed: 25516281]

48. Wickham H. 2009. ggplot2: Elegant Graphics for Data Analysis.

49. Danku J.M.C., Lahner B., Yakubova E., Salt D.E. Plant Mineral Nutrients. Humana Press; Totowa, NJ: 2012. Large-Scale Plant Ionomics; pp. 255–276.

50. Ursache R., Andersen T.G., Marhavý P., Geldner N. A protocol for combining fluorescent proteins with histological stains for diverse cell wall components. Plant J. 2018;93:399–412. [PubMed: 29171896]

51. Pasternak T., Tietz O., Rapp K., Begheldo M., Nitschke R., Ruperti B., Palme K. Protocol: an improved and universal procedure for whole-mount immunolocalization in plants. Plant Methods. 2015;11:50. [PMCID: PMC4625903] [PubMed: 26516341]

Figure 1

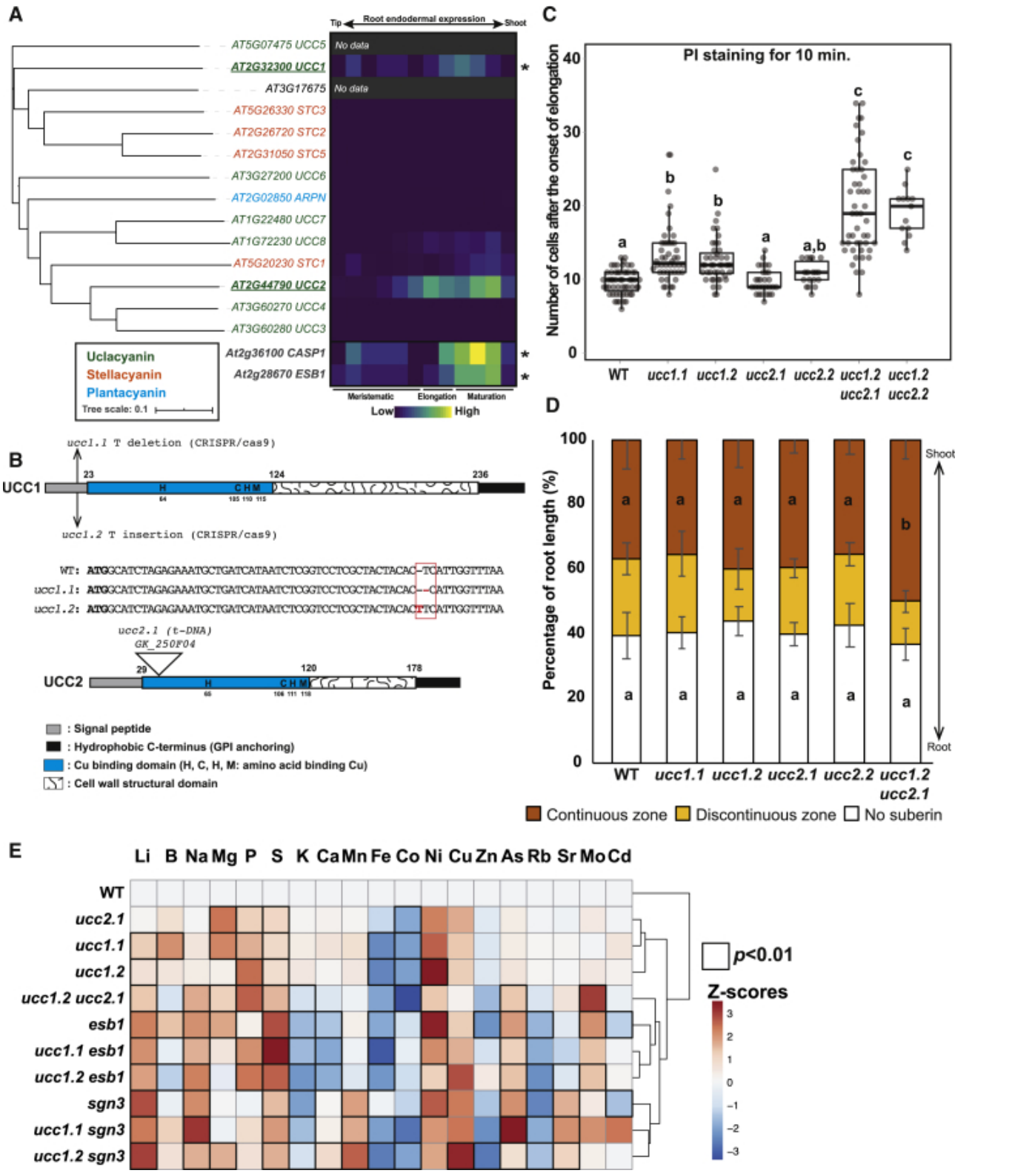

Open in a separate window

Uclacyanins UCC1 and UCC2 Are Required for a Functional Casparian Strip

(A) Left: figure shows a phylogenetic analysis of phytocyanins protein family in *A. thaliana*. The tree was built using the full-length amino acid sequences for all proteins. Different colors represent the three phytocyanins subfamilies: uclacyanins, stellacyanins, and plantacyanins (39). In the tree, branch lengths are proportional to the number of substitutions per site. AT3G17675 has been previously annotated as a stellacyanin (*STC4*), however, the signal peptide for the secretion pathway and the hydrophobic extension for Glycosylphosphatidylinositol (GPI) anchoring are missing. Right: heatmap showing the endodermal expression of the phytocyanins family in *A. thaliana* across the different root zones (Meristematic, Elongation, Maturation). For the analysis, expression data were collected from the Bio-Analytic Resource database, AtGenExpress Consortium. The expression of two endodermal localized proteins, CASP1 and ESB1, were added to the analysis as a reference. Asterisks indicate a significant downregulation in a *myb36* mutant according to [18].

(B) Schematic representation of the UCC1 and UCC2 proteins showing the different protein domains and the types of mutations. Domains were defined according to [19] (see also Figure S1A).

(C) Boxplot analysis showing the number of the cells from the onset of elongation permeable to propidium iodide in wild-type (WT) plants, *ucc1* mutants (*ucc1.1* and *ucc1.2*), *ucc2* mutant (*ucc2.1* and *ucc2.2*), and the double *ucc1 ucc2* mutants (*ucc1.2 ucc2.1* and *ucc1.2ucc2.2*). Data were collected from two independent experiments ($n \geq 29$). Different letters represent significant statistical differences between genotypes using one-way ANOVA and Tukey's test ($p < 0.01$) (see also Figure S1B).

(D) Diagram shows the quantification analysis of the endodermal suberization in roots of WT plants, *ucc1.1*, *ucc1.2*, *ucc2.1, ucc2.2* and *ucc1.2 ucc2.1*. Each color in the graph represents the percentage of the root length (percentage of root length [%]) that is unsuberized (white), discontinuously suberized (yellow), continuously suberized (orange). Suberin was staining with Fluorol yellow 088. ($n \geq 18$). Error bars in the figure are the standard deviation (SD). Different letters represent significant differences between genotypes using a Mann-Whitney test ($p < 0.01$) (See also Figure S1C).

(E) Heatmap representing the ionomic profiles (*Z*-scores) of WT plants, and a collection of mutants with a defective Casparian strip: *ucc2.1*, *ucc1.1*, *ucc1.2*, *ucc1.2 ucc2.1*, *esb1*, *ucc1.1 esb1*, *ucc1.2 esb1*, *sgn3*, *ucc1.1 sgn3*, and *ucc1.2 sgn3* grown in full nutrient conditions on agar plate for 2 weeks ($n = 10$). Elements concentration were determined by ICP-MS and the raw data are available in the Table S1. Significant differences were determined in comparison with WT using a t test ($p < 0.01$). Genotypes were subjected to hierarchical clustering analysis.

Figure 2

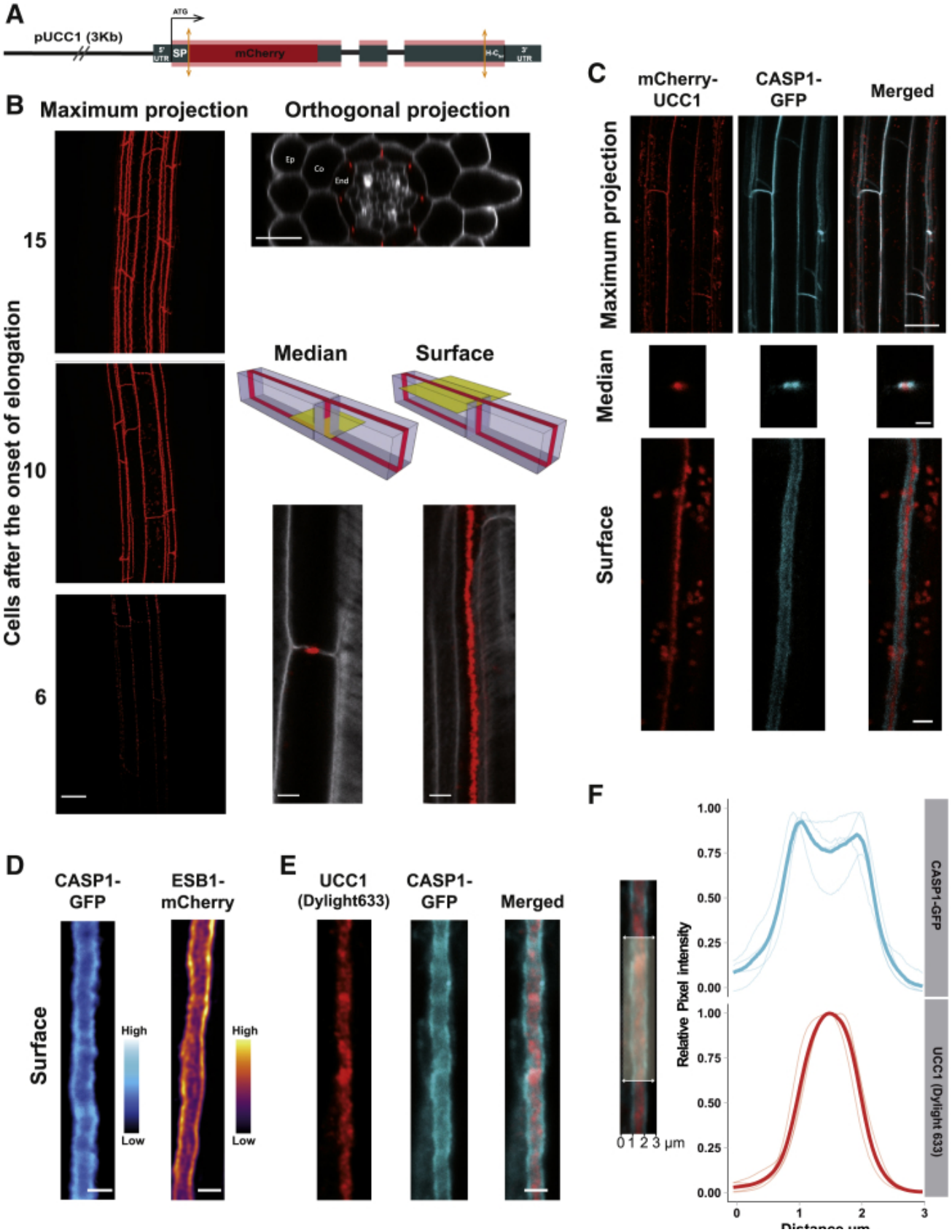

Open in a separate window

UCC1 Defines a New Central Sub-domain in the Casparian Strip

(A) Diagram representing the construct *pUCC1::mCherry-UCC1* (UTR, untranslated region; SP, signal peptide; H C_{ter}, hydrophobic C terminus for GPI anchoring).

(B) Maximum intensity projection, orthogonal, median, and surface views of confocal sections of plants expressing *pUCC1::mCherry-UCC1* (red) in cleared roots. In the case of maximum intensity projection (maximum projection), the figure represents different regions of the root measured as number of cells after the onset of elongation. For the orthogonal, median, and surface views, cell walls were stained with Calcofluor white (gray in the figures). Scale bar, 20 μm for the maximum projection and orthogonal views. Scale bar, 5 μm for the median and surface views. Ep, epidermis; Co, cortex; End, endodermis (see also Figure S2A).

(C) Maximum intensity projection, median, and surface view of confocal sections of plants expressing *CASP1-GFP* (cyan) and *mCherry-UCC1* (red). Signal was captured at the 10^{th} endodermal cell after the onset of elongation observed *in vivo*. Scale bar, 20 μm for maximum projection and 3 μm for median and surface view (see also Figure S2B).

(D) *In vivo* observation of the surface view of an endodermal cell expressing *pESB1::ESB1-mCherry* or *pCASP1::CASP1-GFP*. Scale bar, 2 μm.

(E) Immunolocalization assay of UCC1 protein (red) in plant expressing *pCASP1::CASP1-GFP* (cyan). A primary polyclonal antibody targeting UCC1 was used in combination with a secondary antibody conjugated with Dylight 633. Scale bar, 2 μm see also Figures S2C–S2H.

(F) Graph presenting the distribution of normalized pixels intensity (relative pixel intensity, 0–1) across the Casparian strip (distance in μm) for *CASP1-GFP* fluorescence (cyan) and *UCC1* immunofluorescence (red, Dylight 633). Light curves represent individual replicates coming from individual plants (n = 4). Each replicate is the average pixel intensity across a segment of 25 μm along the Casparian strip axis. Dark curves represent the mean values for *CASP1-GFP* and *UCC1* immunofluorescence.

Figure 3

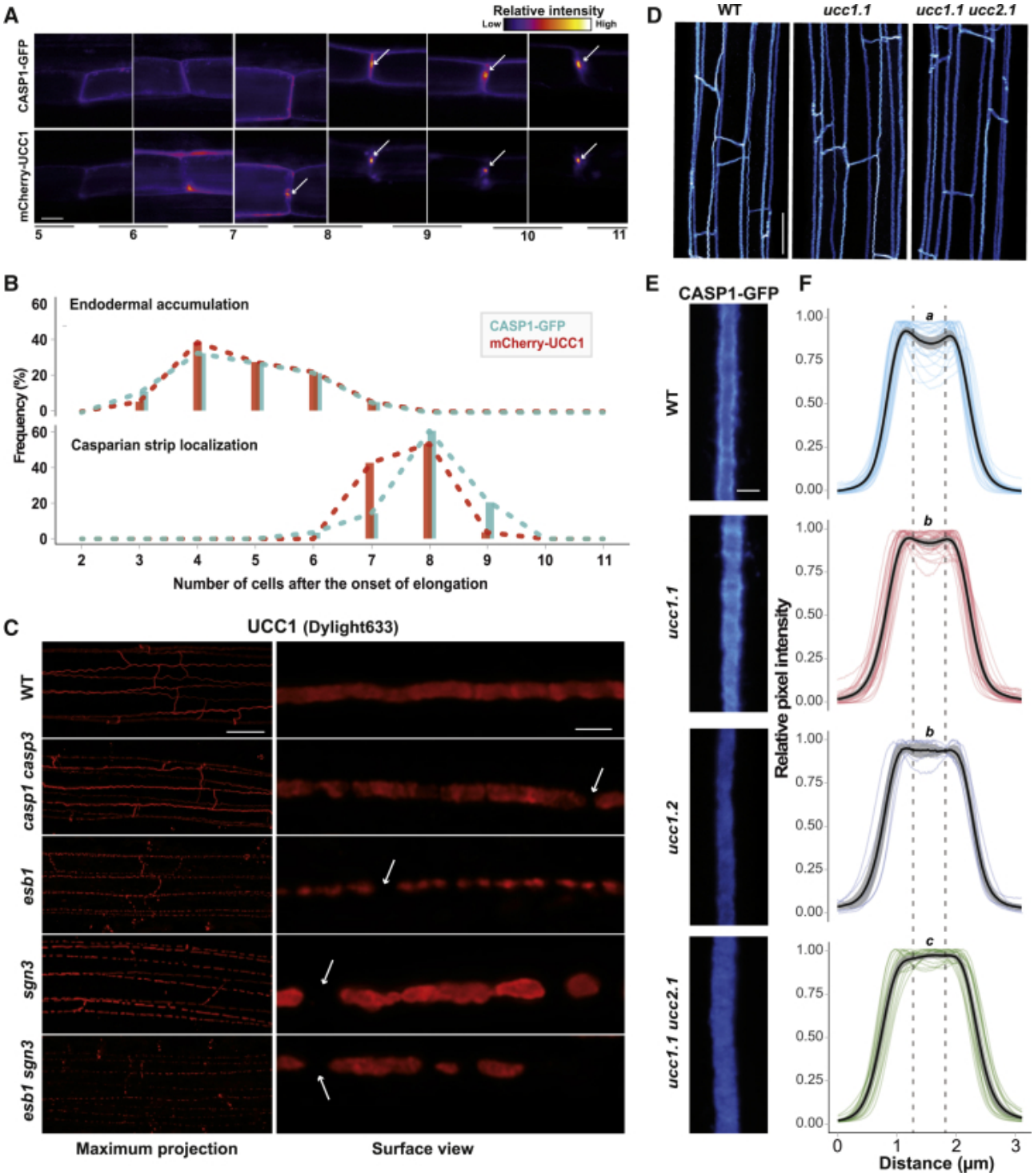

Open in a separate window

Relations between UCC1 Positioning and Other Components of the Casparian Strips Machinery

(A) Analysis of the spatial distribution of CASP1 and UCC1 at the endodermal cell junctions. Images were generated from the same plant co-expressing CASP1-GFP and mCherry-UCC1 using confocal microscopy. The numbers at the bottom of the figure indicate the number of cells after the onset of elongation. White arrows indicate the central accumulation for CASP1-GFP or mCherry-UCC1. Scale bar, 6 µm.

(B) Histograms showing the frequency distribution (Frequency [%]) of the onset of expression (upper plot, n = 18) and the onset of localization at the Casparian strip of CASP1-GFP and mCherry-UCC1 (lower plot, n = 28).

(C) Maximum intensity projection (left) and surface view (right) of UCC1 immunolocalization (red) at 10 cells after the onset of elongation in WT plants and a collection of Casparian strips mutants: *casp1 casp3*, *esb1*, *sgn3*, *esb1 sgn3*. White arrows show gaps in the UCC1 localization. Scale bar, 20 µm for the maximum projections and 2 µm the surface views. see also Figure S3A.

(D) Maximum intensity projection of CASP1-GFP localization in cleared root of WT plants and the mutants *ucc1.1* and *ucc1.1 ucc2.1*. Scale bar, 20 µm.

(E) Surface view of the localization of CASP1-GFP in cleared root of WT plants and the mutants: *ucc1.1*, *ucc1.2*, and *ucc1.1 ucc2.1*. Scale bar, 2 μm.

(F) Quantification of normalized pixels intensity (relative pixel intensity; 0–1) across the Casparian strip in plants expressing CASP1-GFP. The plots are showing the intensity profile for individual replicates ($n \geq 10$), the mean value (black line), and the 95% confidence interval (gray interval). Each replicate corresponds to the quantification of one picture containing a Casparian strip segment of approximately 25 μm long. The pictures were generated at the 15^{th} cells after the onset of elongation from at least 8 individual plants per genotype. Intensity profiles across the Casparian strip were always measured in the same orientation—from the cortical side toward the pericycle side of the endodermis. Letters indicate statistically significant differences between genotypes for the intensity values comprised between the dashed lines using an ANOVA and Tukey's test as post hoc analysis ($p < 0.01$) (see also Figures S3B and S3C).

Figure 4

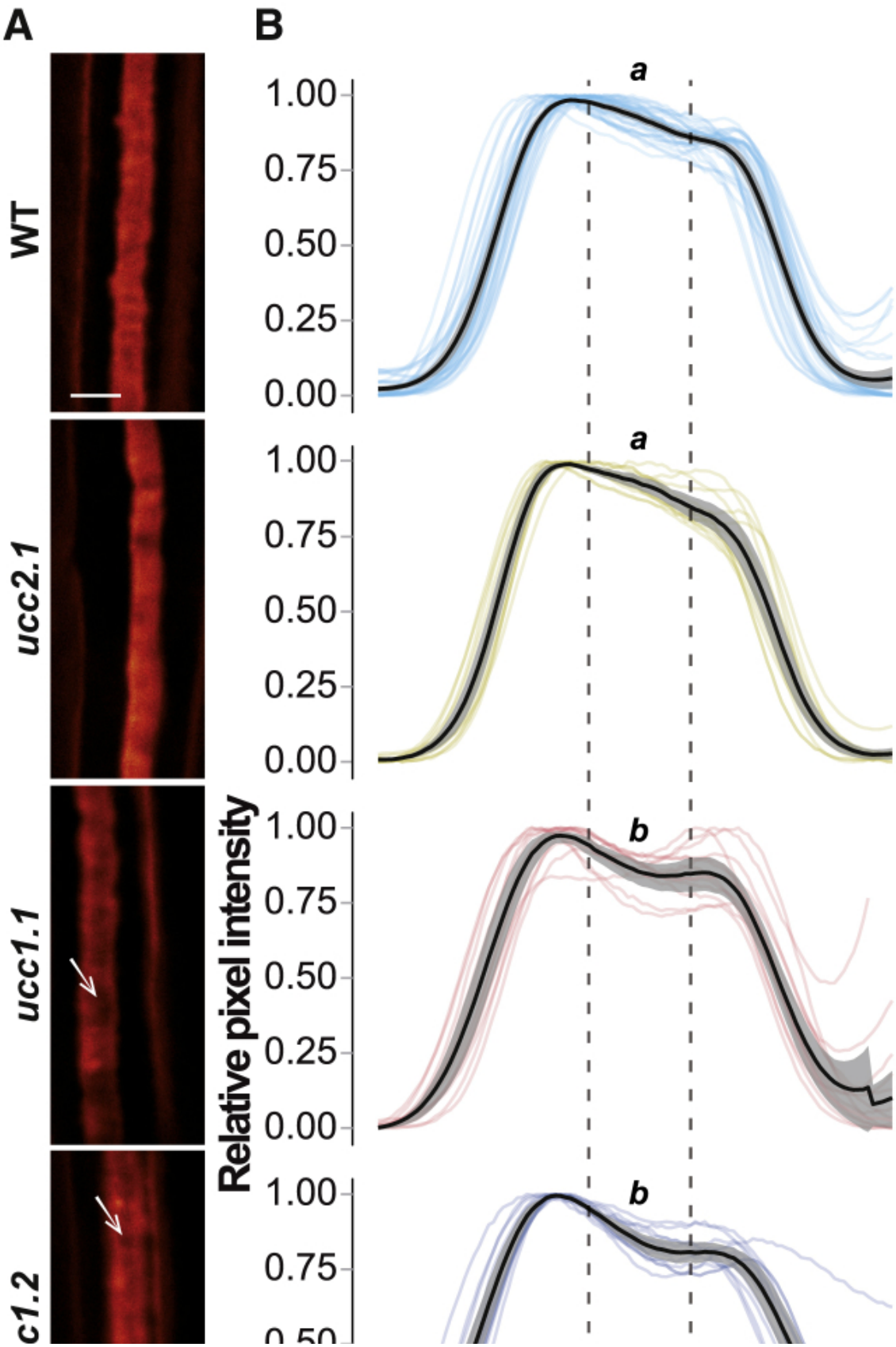

Open in a separate window

UCC1 and UCC2 Are Necessary for the Central Lignification of the Casparian Strip

(A) Surface view of the Casparian strip lignin stained with Basic fuchsin in WT plants and the mutants *ucc2.1*, *ucc1.1*, *ucc1.2*, and *ucc1.2 ucc2.1*. Whites arrows show lack of lignification in the central domain of the Casparian strip across the different genotypes. Scale bar, 2 μm. see also Figure S4A.

(B) Quantification of normalized pixels intensity (0–1) (relative pixel intensity) across the Casparian strip using surface views as shown in (A). The plots show the intensity profile for individual plants ($n \geq 13$). In the figure, the mean value is represented by a black line and the 95% confidence interval is in gray. The data were generated using individual pictures containing a Casparian strip segment of approximately 25 μm long. The pictures were taken at the 15^{th} cells after the onset of elongation and the intensity profiles were measured in the same direction, from the cortex side toward the pericycle side of the endodermis. Letters indicate statistically significant differences between genotypes using an ANOVA and Tukey's test as post hoc analysis ($p < 0.01$) (see also Figure S4B).

REAGENT or RESOURCE	SOURCE	IDENTIFIER
Antibodies		
Rabbit polyclonal anti-UCC1	This paper	N/A
Goat anti-Rabbit IgG (H+L) Secondary Antibody, DyLight 633	Invitrogen	SA5-10034, RRID:AB_2556614
Chemicals, Peptides, and Recombinant Proteins		
MS basal salt mixture, powder	Sigma-Aldrich	M5524
Agar	Sigma-Aldrich	P49805, CAS: 94-53A7921, CASS: 9002-18-01
Piperonylic acid	Sigma-Aldrich	P49805, CAS: 94-53-1
guanidine-HCl	Sigma-Aldrich	G7294
MES	Sigma-Aldrich	M8250 CAS: 1266615-59-1
EDTA	Sigma-Aldrich	EDS, CAS:60-00-4
Phenol:chloroform:isoamylalcohol, 25:24:1	Sigma-Aldrich	P2069
Acetic acid	Sigma-Aldrich	A6283 CAS: 64-19-7
Sodium acetate	Sigma-Aldrich	S2889 CAS, 127-09-3
DNase I, Amplification Grade	Invitrogen	18068015
Nitric acid Primar Plus	Fisher Chemicals	N/2272/PB17 CAS: 7697-37-2
Propidium iodide	Invitrogen	P1304MP, CAS: 25535-16-4
Calcofluor White	Polysciences,	CAT#4359
Basic Fuchsin	Fluka, Analytical	CAS: 58969-01-0
Auramine-O	Sigma-Aldrich	SLA 1027 CAS: 2465-27-2
paraformaldehyde	Sigma-Aldrich	P6148, CAS:3052-89-4
xylitol	Sigma-Aldrich	W507930, CAS: 87-99-0
Sodium deoxycholate	Sigma-Aldrich	D6750, CAS: 302-95-4
urea	Sigma-Aldrich	U5378, CAS:57-13-6
Fluorol Yellow 088	Santa Cruz Biotechnology	SC215052, CAS: 81-37-8
PIPES	Sigma-Aldrich	P-3768, CAS: 76836-02-7
EGTA	Sigma-Aldrich	E3889, CAS: 67-42-5
$MgSO_4 \cdot 7H_2O$	Sigma-Aldrich	63138, CAS:10034-99-8
KOH	Sigma-Aldrich	P5958, CAS:1310-58-3
Methanol	Sigma-Aldrich	82762, CAS:67-56-1

Open in a separate window